KSOE

Journal of Ocean Engineering and Technology 37(4), 164-171, August, 2023
https://doi.org/10.26748/KSOE.2023.012

pISSN 1225-0767
eISSN 2287-6715

Original Research Article

Study on the Vibration Characteristics of Yaw Gear System for Large-Capacity Offshore Wind Turbine

HyoungWoo Lee[1], SeoWon Jang[2] and Seok-Hwan Ahn[3]

[1]*Professor, Department of Unmanned Aero Mechanical Engineering, Jungwon University, Goesan, Korea*
[2]*Graduate Student, Department of Convergence Engineering, Jungwon University, Goesan, Korea*
[3]*Professor, Department of Unmanned Aero Mechanical Engineering, Jungwon University, Goesan, Korea*

KEYWORDS: Yaw gear system, Natural frequency, Critical speed, Campbell diagram, Load duration distribution

ABSTRACT: *Vibration and noise must be considered to maximize the efficiency of a yaw system and reduce the fatigue load acting on a wind turbine. This study investigated a method for analyzing yaw-system vibration based on the change in the load-duration distribution (LDD). A substructure synthesis method was combined with a planetary gear train rotational vibration model and finite element models of the housing and carriers. For the vibration excitation sources, the mass imbalance, gear mesh frequency, and bearing defect frequency were considered, and a critical speed analysis was performed. The analysis results showed that the critical speed did not occur within the operating speed range, but a defect occurred in the bearing of the first-stage planetary gear system. It was found that the bearing stiffness and first natural frequency increased with the LDD load. In addition, no vibration occurred in the operating speed range under any of the LDD loads. Because the rolling bearing stiffness changed with the LDD, it was necessary to consider the LDD when analyzing the wind turbine vibration.*

1. Introduction

A wind turbine typically consists of a blade rotor that transfers the received energy to a generator, a power transfer unit, a nacelle in which the generator and various electrical and mechanical devices are installed, and a tower that supports the weight of the nacelle assembly and load delivered through the blade (Hong et al., 2006). Because even a single malfunction of a wind-power generation system can induce significant economic and social losses, only products that can guarantee at least 20 years of service life can enter the commercial market. In addition to the increase in the size of the system, consideration must be given to vibration, noise, and weight reduction when designing a gearbox because a service life of at least 20 years must be guaranteed (Lee and Kang, 2014).

A yaw system maximizes the system efficiency and reduces the fatigue load acting on a wind turbine by positioning the rotor and nacelle so that they face in the direction that the wind is blowing. The vibration and noise of the yaw system must be taken into account because a wind turbine must be guaranteed a service life of at least 20 years. Accordingly, continuous research has been conducted on the vibration and noise of rotary machines. Itoh studied a method of using a damped free vibration mode shape for systems with complex structures (Itoh, 1973). Kahraman et al. (1992) calculated the critical speed considering the torsion of a gear and coupled effects of bending vibration, and found the response for an unbalanced mass and transmission error using a finite element method. To analyze the response of a planetary gear train using the finite element method, Parker et al. (2000) designed a finite element model of a planetary gear train and analyzed the dynamic response and unique characteristics such as the natural frequency and vibration modes. Dong et al. (2015) researched non-linear dynamic modeling, including torsion modeling, in order to examine the vibration characteristics of a planetary gear. Wang and Morse (1972) performed static and dynamic torsion response analyses of a general gear train system using a transfer matrix method. Choy et al. (1991) analyzed the steady state response by developing a three-stage spur gear system model that included the torsion of a gear train. To improve the analysis techniques for complex planetary gear systems considering various types of frictions, Tanaka analyzed the characteristics of a planetary gear in the form of a matrix by finding system equations from element equations, corresponding to the finite element method (FEM) (Tanaka, 1984). Iida et al. (1980) claimed that a gear train model yielded different results depending on

Received 10 May 2023, revised 6 July 2023, accepted 19 July 2023
Corresponding author Seok-Hwan Ahn: +82-43-830-8942, shahn@jwu.ac.kr

whether the dynamic coupling of a spur gear was considered. Bossanyi studied a method for controlling the torque applied to the yaw to balance the energy according to the load and for individually controlling the yaw system to reduce loads applied asymmetrically (Bossanyi, 2005). Prohl proposed a transfer matrix model of a gear train, and analyzed the critical speed, dynamic response, and unique characteristics of this gear train supported by a bearing based on the transfer matrix method (Prohl, 1945).

The aforementioned studies performed vibration analyses only for a gear train without considering the finite element models of the housing and carriers. Therefore, there is a need for a vibration analysis that considers a finite element model of the housing and gear, as well as the planetary gear train.

This study examined the vibration characteristics of the yaw system for a large-capacity wind turbine, and proposed a method for performing a vibration analysis of the yaw system by combining finite element models of the housing and carriers with a rotor vibration model of the planetary gear train using a substructure synthesis method. Furthermore, the characteristics were analyzed by comparing the natural frequency results with and without consideration given to the finite elements of the housing and carriers. The vibration excitation sources for the bearing defect error, gear mesh frequency, and mass imbalance acting on the yaw system were modeled, and the critical speed was analyzed to determine the resonance within the scope of the operation speed range.

2. Vibration Modeling and Vibration Characteristic Analysis of the Yaw System

2.1 Vibration Modeling of the Yaw System

In this study, modeling was performed using an 8-MW yaw decelerator model. The vibration model of the yaw system was designed using MASTA 12.1, which is a gear analysis program. Fig. 1 shows the vibration model of the yaw system, which consisted of a four-stage planetary gear system. The output axis of each stage, when a ring gear was fixed, was connected to the subsequent input axis through a spline. The power of a motor input through the first sun gear was delivered to the output axis through the second, third, and fourth planetary gear systems.

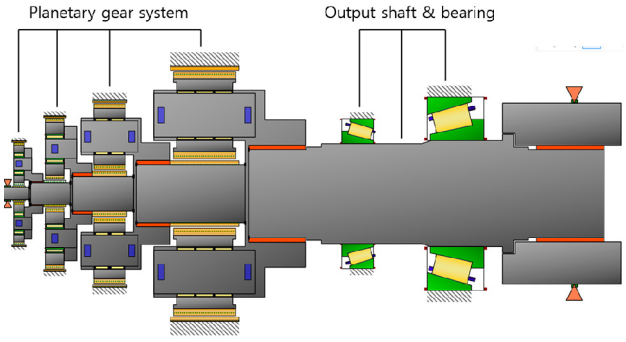

Fig. 1 Two-dimensional vibration model of yaw gear system

Table 1 Planetary information for 1st stage of yaw gear system

Stage 1	Sun	Planetary	Ring
Planetary gear		3	
Module		1.75	
Pressure angle (°)		20	
Number of teeth	14	39	94
Center distance (mm)		47.6	
Reduction ratio		7.714	

Table 2 Planetary information for 2nd stage of yaw gear system

Stage 2	Sun	Planetary	Ring
Planetary gear		3	
Module		2.5	
Pressure angle (°)		25	
Number of teeth	17	39	97
Center distance (mm)		71.7	
Reduction ratio		6.706	

Table 3 Planetary information for 3rd stage of yaw gear system

Stage 3	Sun	Planetary	Ring
Planetary gear		4	
Module		3.5	
Pressure angle (°)		25	
Number of teeth	21	30	83
Center distance (mm)		91.4	
Reduction ratio		4.952	

Table 4 Planetary information for 4th stage of yaw gear system

Stage 4	Sun	Planetary	Ring
Planetary gear		4	
Module		5	
Pressure angle (°)		25	
Number of teeth	21	28	79
Center distance (mm)		125.5	
Reduction ratio		0.950	

Detailed specifications of the four stages of the planetary gear system are presented in Tables 1, 2, 3, and 4, respectively. The reduction ratios of the planetary gear system were 7.714 in stage 1, 6.706 in stage 2, 4.952 in stage 3, and 0.95 in stage 4; the overall reduction ratio was approximately 1,219.96, with the 1,158.961 rpm rotational speed of the motor input in the first sun gear decelerated to 0.47 rpm.

2.2 Vibration Characteristic Analysis of the Yaw System

Most structural analyses are performed based on the finite element method, but an extensive amount of time is required for computing and dividing the mesh for large structures. To overcome this drawback, the

entire structure was divided into several elements, and then each modal variable was independently determined for each element. The elements were then synthesized using geometric suitability conditions for the elements as constraint conditions as part of the substructure synthesis method to find the modal variable, stress, and strain of the structure (Choi et al., 1989).

MASTA 12.1 was used for the rotor-vibration modeling of the yaw system gear train, and then the ANSYS 22 finite element models of the housing and carriers were connected through the substructure synthesis method. Fig. 2 shows the finite element model of the housing that was produced using ANSYS 22. Because the teeth of the ring gear were included in the MASTA 12.1 vibration model, they were excluded from the finite element model. If the mesh quality of a finite element model is poor when synthesizing it with the gear train model using MASTA 12.1, a matrix cannot be formed and an error occurs. Accordingly, the bolt holes of the ring gear, flange, and output housing were deleted when forming the mesh in order to improve the mesh quality. The finite element model consisted of 191,948 nodes and 744,424 elements.

Fig. 3 shows the part where the gear train and housing node are connected. The output axis bearing of the gear train is in contact with

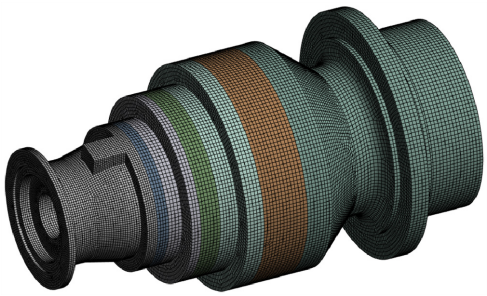

Fig. 2 Finite element model of housing

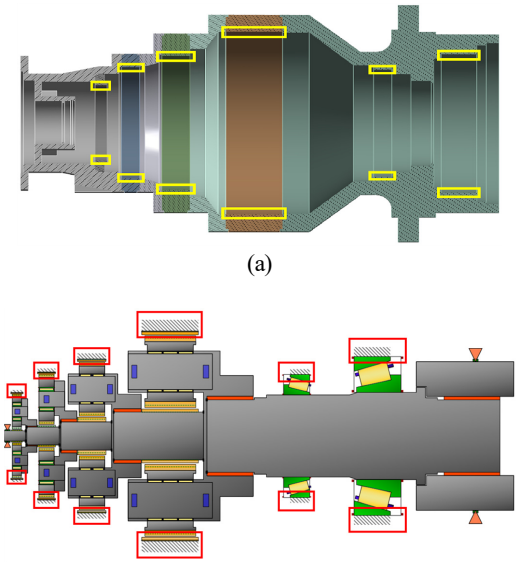

(a) (b)

Fig. 3 Housing and gear train connection parts: (a) housing connection part and (b) gear train connection part

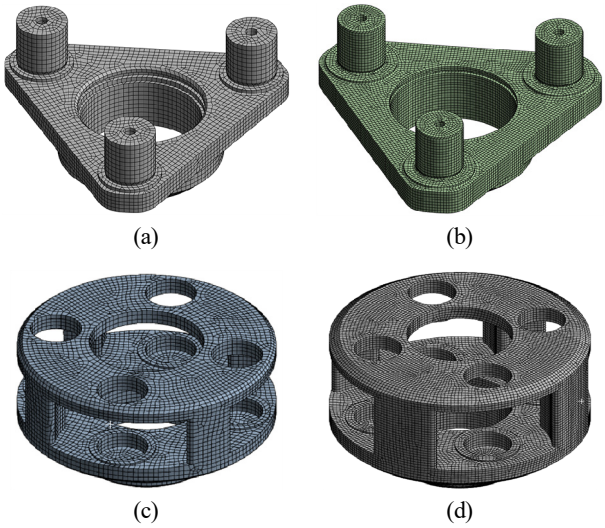

(a) (b) (c) (d)

Fig. 4 Carrier finite element models: (a) 1st carrier, (b) 2nd carrier, (c) 3rd carrier, and (d) 4th carrier

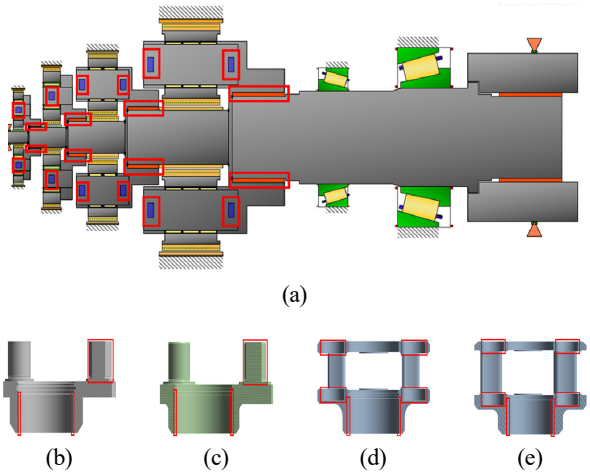

(a) (b) (c) (d) (e)

Fig. 5 Carrier and gear-train connection parts: (a) gear train, (b) 1st carrier, (c) 2nd carrier, (d) 3rd carrier, and (e) 4th carrier

the output housing, and the ring gear of each stage is connected with the ring gear of the housing.

Fig. 4 shows the finite element models of the carriers devised to be synthesized with the gear train model. The finite element model of the first carrier has 82,866 nodes and 23,228 elements, that of the second carrier has 253,896 nodes and 69,742 elements, that of the third carrier has 159,828 nodes and 46,432 elements, and that of the fourth carrier has 597,403 nodes and 163,068 elements.

Fig. 5 shows the part where the gear train and carriers are connected. The substructure synthesis of the carriers involves connecting each carrier with the node of the part contacting the planetary pin, and connecting the node of the spline at which the carrier is connected to the subsequent stage.

Fig. 6(a) shows the vibration model when only the gear train is considered, without considering the finite element models of the housing and carriers. Fig. 6(b) shows the vibration model when the

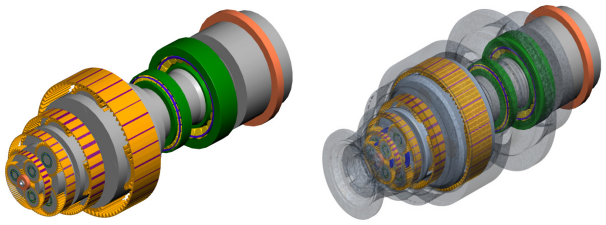

(a) (b)

Fig. 6 Natural frequency comparison models: (a) vibration model without finite element mode and (b) vibration modeling with infinite element mode

Table 5 Comparison of natural frequency analysis results

Mode	Natural frequency (Hz)	
	without finite element model	with finite element model
1	100.76	104.83
2	105.88	108.29
3	275.08	184.57
4	292.33	203.04
5	296.21	233.14
6	411.91	313.96

finite element models of the housing and carriers are synthesized with the planetary gear train using the substructure synthesis method. Table 5 presents a comparison of the natural frequencies in cases where the finite element models of the housing and carriers were and were not taken into consideration, under the condition that the torque was the largest among the load duration distribution (LDD) data. The natural frequency of the case where the finite element models of the housing and carriers were taken into consideration was lower than that where they were not taken into consideration.

3. Vibration Excitation Source Modeling and Critical Speed Analysis of the Yaw System

3.1 Modeling of the Vibration Excitation Source

The excitation sources applied to the yaw system included the mass imbalance, gear mesh frequency, and errors in the bearing installation. The gear mesh frequency is primarily caused by gear-teeth machining errors and system deformation due to loads, and is expressed as the product of the rotational speed and number of gear teeth. Mass imbalance occurs when there is an eccentric mass caused by machining errors, and is identical to the rotational speed. The types of excitation frequencies due to rolling-bearing defects include the fundamental train frequency (FTF), ball spin frequency (BS), outer racer frequency (OR), and inner racer frequency (IR) (Lee, 1999).

Table 6 presents the bearing characteristics of each stage, while Table 7 presents the excitation frequency ratio considering the mass imbalance and gear mesh frequency of the yaw system. Here, 1X indicates the changes in the rotational speed input in the first sun gear. The excitation sources related to bearing defects are listed in Table 8.

Table 6 Rolling bearing information

Stage	1	2	3	4	Ouput left	Output right
Number of ball	15	19	26	30	31	21
Pitch diameter	29	39	54	74	200.328	239.942
Ball diameter	4	4	4	4	19.153	34.335
Contact angle	0	0	0	0	17	16.1722

Table 7 Excitation frequency of mass imbalance and gear mesh frequency

Excictation source	Excitation frequency ratio		
		Sun	Planetary
Mass imbalance	Stage 1	1X	0.13X
	Stage 2	0.13X	0.019X
	Stage 3	0.019X	0.004X
	Stage 4	0.004X	0.001X
Gear mesh frequency	Stage 1	14X	
	Stage 2	2.204X	
	Stage 3	0.406X	
	Stage 4	0.082X	

Table 8 Excitation frequency ratio of bearing

Stage	1	2	3	4	Ouput left	Output right
FTF	1.073X	0.166X	0.034X	0.007X	0.008X	0.009X
BS	8.857X	1.791X	0.503X	0.145X	0.082X	0.054X
OR	16.104X	3.166X	0.902X	0.223X	0.25X	0.187X
IR	21.257X	3.89X	1.047X	0.249X	0.237X	0.144
rps	2.49	0.37	0.075	0.015	0.002	0.015

3.2 Critical Speed Analysis

Vibration and noise occur in the yaw system of a wind turbine when the excitation frequency and natural frequency of the yaw system are identical. If the excitation frequency is γ_i, where $i = 1, 2, 3, \cdots, N$, and the natural frequency of the yaw system is λ_i, where $i = 1, 2, 3, \cdots, N$, resonance occurs when $\gamma_i = \lambda_i$. If the excitation frequency is $\gamma_i = c_i \omega_{cr}$, critical speed ω_{cr} becomes $\omega_{cr} = \lambda_i / c_i$. Here, c_i is the coefficient of the excitation frequency (Kim et al., 2011).

The input speed of the yaw system was 1,158.96 rpm; Tables 6 and 8 present the excitation sources with respect to changes in the input speed. Figs. 7 and 8 show Campbell diagrams of the mass imbalance, gear mesh frequency, and bearing defects (FTF, BS, OR, IR).

Figs. 7–14 show that the critical speed of the mass imbalance, gear mesh frequency, and bearing defects did not occur within the operation speed (1,158.96 rpm) range.

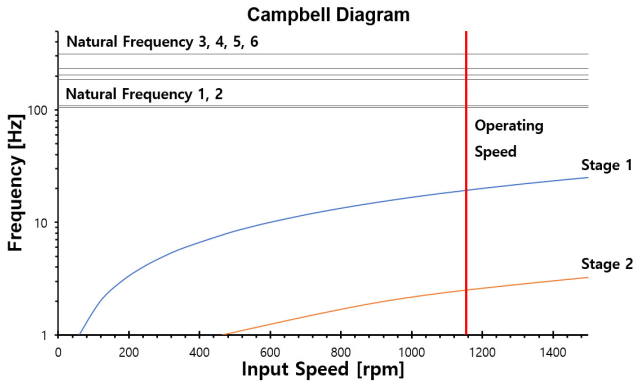

Fig. 7 Campbell diagram of mass unbalance

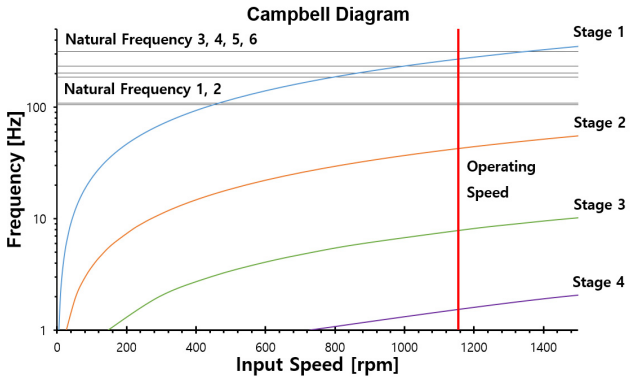

Fig. 8 Campbell diagram of gear mesh frequency

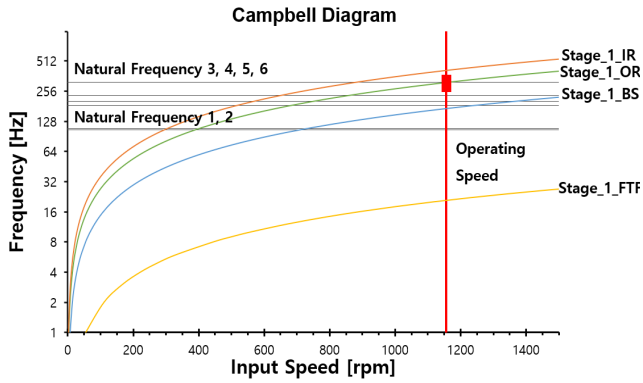

Fig. 9 Campbell diagram of stage 1 bearing

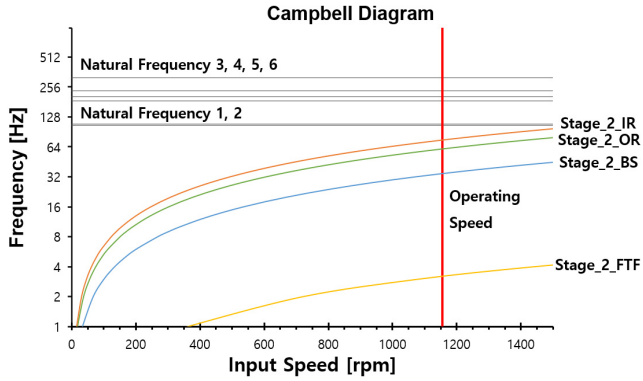

Fig. 10 Campbell diagram of stage 2 bearing

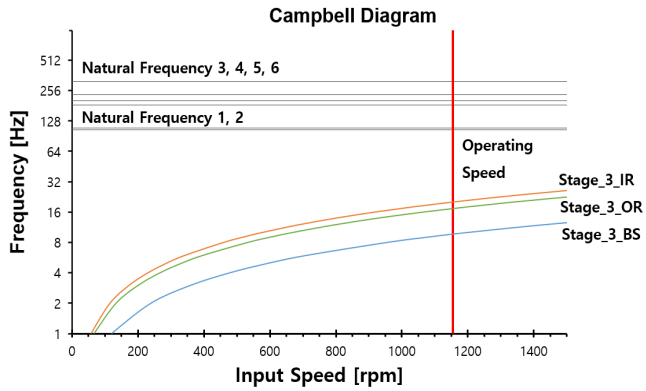

Fig. 11 Campbell diagram of stage 3 bearing

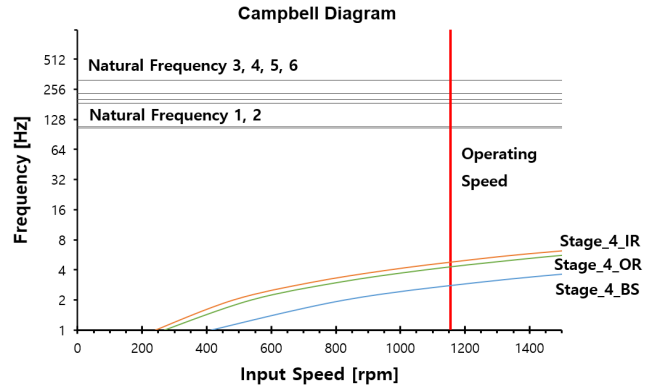

Fig. 12 Campbell diagram of stage 4 bearing

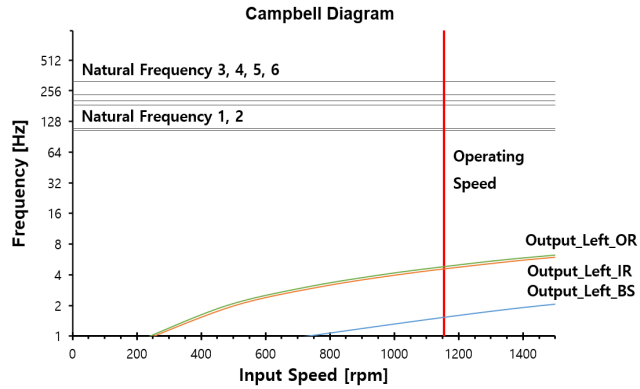

Fig. 13 Campbell diagram of output left bearing

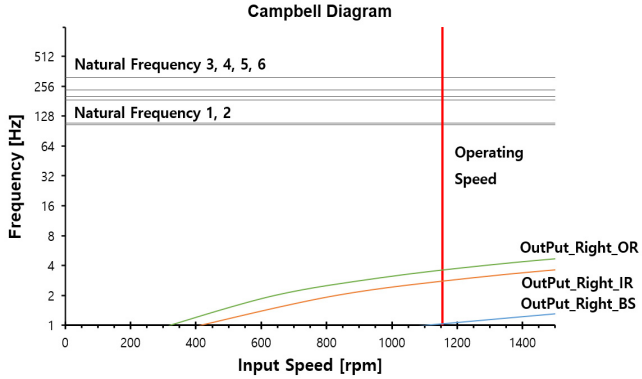

Fig. 14 Campbell diagram of output right bearing

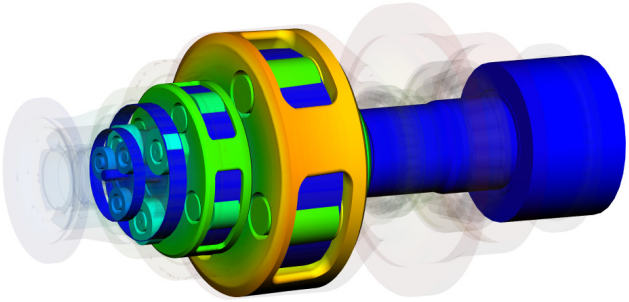

Fig. 15 Mode shape of mode 6

Fig. 9 presents the Campbell diagram of the stage 1 planetary gear, where the bearing outer ring of the first planetary gear coincides with the natural frequency of mode 6, as listed in Table 6; the mode shape of the sixth natural frequency is illustrated in Fig. 15. According to the mode shape results, a large vibration mode occurred in the vertical direction of the first planetary gear, which indicated that the bearing condition of the first planetary gear requires regular inspections.

4. Natural Frequency Characteristic Analysis with Respect to Changes in the LDD

The mathematical model of the vibration system of a wind turbine yaw system can be expressed as shown in Eq. (1).

$$[M]\ddot{q}+[C]\dot{q}+[K]q=0 \tag{1}$$

$$\{q\} = \begin{Bmatrix} x \\ y \\ z \\ \theta_x \\ \theta_y \\ \theta_z \end{Bmatrix} \tag{2}$$

Here, $[M]$ is the system mass matrix, $[C]$ is the system damping matrix, $[K]$ is the system stiffness matrix, and q is the system response (Min et al., 2015).

Eq. (2) expresses the torsion, rotational, and bending direction vectors, along with the three displacement vectors of x, y, and z.

A general industrial gear box receives a fairly constant load. The vibration analysis of a wind turbine must consider various types of LDDs. The rolling bearing stiffness of a wind turbine gear box varies depending on the applied torque; thus, further research is needed on the effects of changes in the LDD on the first natural frequency.

Because there is a lack of research on the changes in the characteristics of the natural frequency with respect to changes in the LDD, this system found the natural frequency of the yaw system in terms of changes in the LDD.

Figs. 16 and 17 illustrate the changes in the natural frequency with respect to the bearing stiffness when the largest load (116,320 Nm) of the LDD was considered to be one, and the load was increased in 10% increments from 10% of the largest load to 100%.

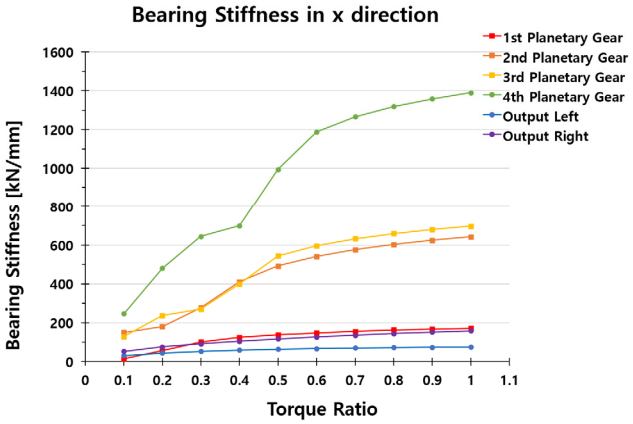

Fig. 16 Variation of bearing stiffness in x-direction according to load

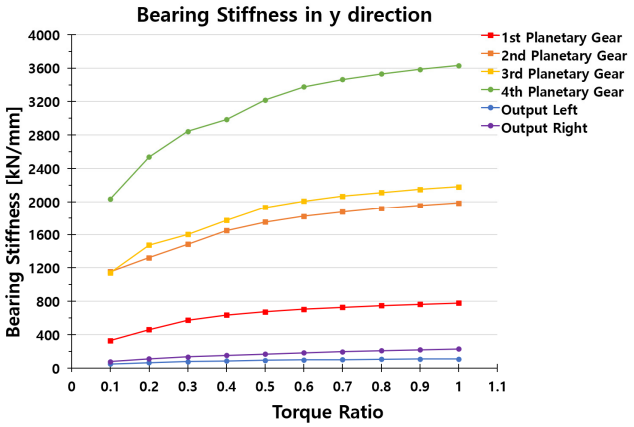

Fig. 17 Variation of bearing stiffness in y-direction according to load

Table 9 Changes in x-direction bearing stiffness according to load

Torque (Nm)	1	2	3	4	Ouput left	Output right
11,632	14.8	149.5	129.5	247.2	31.4	53.2
23,264	56.6	180.4	237.1	480.2	44.5	75.7
34,896	101.6	277.1	270.2	643.6	53.5	91.9
46,528	124.1	411.2	399.6	698.9	59.9	105
58,160	137.9	492	543.2	994.2	64	116.3
69,792	148	541	596	1187.6	67.4	126.4
81,424	155.8	575.8	641.6	1266	70.3	135.5
93,056	163.2	602.6	658.4	1318.9	72.5	143.9
104,688	167.5	624.3	679.4	1358.6	74	151.7
116,320	172.0	642.1	696.6	1389.6	75.3	159

Fig. 16 shows the stiffness variation in the x-direction of a bearing in each stage according to changes in the load. The stiffness in the x-direction varied significantly with respect to the load.

Fig. 17 shows the stiffness variation in the y-direction of a bearing in each stage according to changes in the load. The stiffness in the

Table 10 Changes in y-direction bearing stiffness according to load

Torque (Nm)	1	2	3	4	Ouput left	Output right
11,632	328.2	1154.8	1141.4	2036.3	48.6	78.6
23,264	459.4	1322.7	1473.8	2537	64.5	110.3
34,896	573.9	1483.2	1602.9	2844.4	77	133.1
46,528	634.7	1647.4	1770.8	2985.7	86.2	151.7
58,160	674.5	1751.6	1930.3	3218	92.4	167.9
69,792	704.7	1821.5	2008	3376.3	97.5	182.3
81,424	728.6	1874.9	2066.4	3462.8	101.8	195.3
93,056	748.2	1918.1	2112.2	3529.2	105.1	207.2
104,688	764.7	1954.6	2149.5	3583.9	107.5	218.5
116,320	779	1985.6	2180.9	3630.3	109.4	228.9

y-direction also varied significantly with respect to the load. The detailed numerical values shown in Figs. 16 and 17 are presented in Table 9 and Table 10, respectively.

Fig. 18 shows the variations in the first natural frequency with respect to the load. Because the lowest first natural frequency was 72.186 Hz, exceeding the operation speed of 1,158.96 rpm (19.316 Hz), all the LDD data were safely within the range of the operation speed. The detailed numerical values shown in Fig. 18 are presented in Table 11.

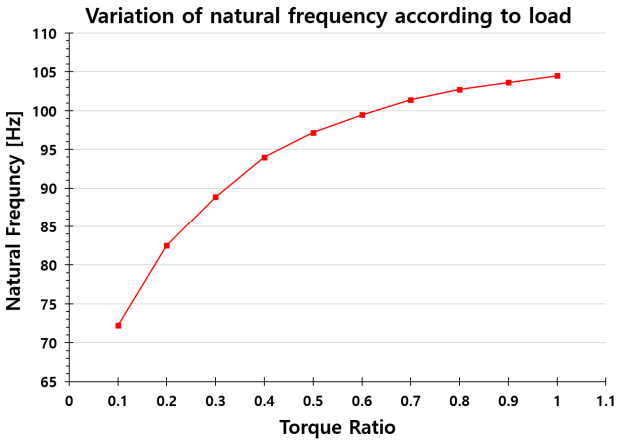

Fig. 18 Variation of natural frequency according to load

Table 11 Changes in natural frequency according to load

Torque (Nm)	Natural frequency (Hz)
11,632	72.1
23,264	82.5
34,896	88.8
46,528	93.9
58,160	97.1
69,792	99.4
81,424	101.3
93,056	102.7
104,688	103.6
116,320	104.4

5. Conclusion

This study investigated a method for combining finite element models of the housing and carriers with the rotor vibration model of a planetary gear train through substructure synthesis and analyzing the vibration of the yaw system with respect to variations in the LDD.

When the natural frequencies were compared for cases where the finite elements of the housing and carriers were and were not considered, the natural frequency was lower in the case where the finite element models were taken into consideration. In addition, the critical speed of the yaw system was analyzed by modeling the vibration excitation sources for the mass imbalance, gear mesh frequency, and bearing defect frequency applied to the yaw system, and the results demonstrated that the critical speed of the mass imbalance and gear mesh frequency did not occur within the operation-speed range. However, the bearing condition must be inspected periodically because the outer ring of the first planetary gear bearing coincided with the sixth natural frequency (313.96 Hz) in the critical speed analysis of the bearing installation error.

When the LDD was increased in 10% increments from 10% of the largest load to 100%, both the bearing stiffness and first natural frequency increased with the LDD. Furthermore, the first natural frequency was 72.186 Hz for the lowest LDD, which exceeded the operation speed of 1,158.96 rpm (19.316 Hz); thus, according to the changes in the LDD, the vibration did not occur within the operation-speed range. Because the rolling bearing stiffness varied with the LDD, further analysis of the vibration of a wind turbine must be performed while considering the LDD.

Conflict of Interest

Seok-Hwan Ahn serves as an editorial board member of the Journal of Ocean Engineering and Technology, but he had no role in the decision to publish this article. No potential conflict of interest relevant to this article was reported.

Funding

This thesis is research of a study conducted with the support of the ‘Renewable Energy Core Technology Development Project’ supported by the Korea Energy Technology Evaluation and Planning. (No. 20213030020020)

References

Bossanyi, E. A. (2005). Further load reductions with individual pitch control. *Wind Energy, 8*(4), 481–485. https://doi.org/10.1002/

we.166

Choi, J. W., Lee, S. S., & Park. Y. S. (1989). A review of mode synthesis techniques and its application between FE and experimental Model. *Transactions of the Korean Society of Mechanical Engineers, 13*, 799−806. https://doi.org/10.22634/KSME.1989.13.4.799

Choy, F. K., Tu, Y. K., Savage, M., & Townsend, D. P. (1991). Vibration signature and modal analysis of multi-stage gear transmission. *Journal of the Franklin Institute, 328*(2), 281−298. https://doi.org/10.1016/0016-0032(91)90035-2

Dong, H., Zhang, K., Wang, D., Wu, Y., & Bai, S. (2015). Dynamic modeling of planetary gear train for vibration characteristic analysis. *Mechanisms Trasmissions and Application, 31*, 187−195. https://doi.org/10.1007/978-3-319-17067-1_20

Hong, H. S., Park, J. I., Bang, J. H., Ryu, J. Y., & Kim, D. H. (2006). Research for 2MW wind turbine tower shell design optimization. *The Korean Society for New and Renewable Energy, 2*(4), 19−26.

Iida, H., Tamura, T., Kikuchi, K., & Agata, H. (1980). Coupled torsional-flexural vibration of a shaft in a geared system of rotors. *Bulletin of JSME, 23*(186), 2111−2117. https://doi.org/10.1299/jsme1958.23.2111

Itoh, T. (1973). Damped vibration mode superposition method for dynamic response anaylsis. *Earthquake Engineering Structural Dynamics, 2*(1), 47−57. https://doi.org/10.1002/eqe.4290020105

Kahraman, A., Ozguven, H. N., Houser, D. R., & Zakrajsek, J. J. (1992). Dynamic analysis of geared rotors by finite elements. *Journal of Mechanical Design, 114*(3), 507−514. https://doi.org/10.1115/1.2926579

Kim, J. S., Lee. H. W., Park, N. G., Kim, Y. D., Kim, S. Y., & Lee, D. H. (2011). Characteristic of vibration in wind turbine system. *Journal of the Korean Society of Marine Engineering, 35*(6), 786−795. https://doi.org/10.5916/jkosme.2011.35.6.786

Lee, H. Y. (1999). *An analytical investigation on vibrational characteristics of multi-mesh geared system using transfer aatrix method* [Master's thesis, Busan University].

Lee, H. Y., & Kang, D. K. (2014). Gear teeth modification for a 2.5MW wind turbine gearbox. *Journal of the Korean Society of Manufacturing Technology Engineers, 23*(2), 109−117. https://doi.org/10.7735/ksmte.2014.23.2.109

Min, Y. S., & Lee, H. W. (2015). A study on the design of cycloidal pitch reducer for the 2MW-class wind turbine. *Journal of the Korean Society of Marine Engineering, 39*(9), 895−902. https://doi.org/10.5916/jkosme.2015.39.9.895

Parker, R. G., Agashe, V., & Vijayakar, S. M. (2000). Dynamic response of a planetary gear system using a finite element/contact mechanics model. *Journal of Mechanical Design, 122*(3), 304−310. https://doi.org/10.1115/1.1286189

Prohl, M. A. (1945). A general method for calculating critical speeds of flexible rotors. *Journal of Applied Mechanics, 12*(3), 142−148. https://doi.org/10.1115/1.4009455

Tanata, M. (1984). Matrix methods in planetary gear train analyses. *Society of Automotive Engineers, 93*(5), 333−340. https://www.jstor.org/stable/44721481

Wang, S. M., & Morse. JR. I. E. (1972). Torsional response of a gear train system. *Manfacturing Science and Engineering, 94*(2), 583−592. https://doi.org/10.1115/1.3428200

Author ORCIDs

Author name	ORCID
Lee, HyoungWoo	0000-0002-7312-6910
Jang, SeoWon	0009-0000-7042-9644
Ahn, Seok-Hwan	0000-0002-9598-9995